Applied Physics Letters

# Epitaxial $L1_0$-FeNi films with high degree of order and large uniaxial magnetic anisotropy fabricated by denitriding FeNiN films

Cite as: Appl. Phys. Lett. **116**, 242404 (2020); https://doi.org/10.1063/5.0011875
Submitted: 25 April 2020 • Accepted: 01 June 2020 • Published Online: 15 June 2020

Keita Ito, Masahiro Hayashida, Hiroto Masuda, et al.

Applied Physics Letters ARTICLE scitation.org/journal/apl

# Epitaxial $L1_0$-FeNi films with high degree of order and large uniaxial magnetic anisotropy fabricated by denitriding FeNiN films

Cite as: Appl. Phys. Lett. **116**, 242404 (2020); doi: 10.1063/5.0011875
Submitted: 25 April 2020 · Accepted: 1 June 2020 ·
Published Online: 15 June 2020



Keita Ito,[1,2,a)] Masahiro Hayashida,[1] Hiroto Masuda,[1] Takahiro Nishio,[3] Sho Goto,[3] Hiroaki Kura,[3] Tomoyuki Koganezawa,[4] Masaki Mizuguchi,[1,2] Yusuke Shimada,[1] Toyohiko J. Konno,[1] Hideto Yanagihara,[5] and Koki Takanashi[1,2,6]

## AFFILIATIONS

[1]Institute for Materials Research, Tohoku University, Sendai 980-8577, Japan
[2]Center for Spintronics Research Network, Tohoku University, Sendai 980-8577, Japan
[3]Advanced Research and Innovation Center, DENSO CORPORATION, Nisshin, Aichi 470-0111, Japan
[4]Japan Synchrotron Radiation Research Institute, SPring-8, Sayo, Hyogo 679-5198, Japan
[5]Department of Applied Physics, University of Tsukuba, Tsukuba, Ibaraki 305-8573, Japan
[6]Center for Science and Innovation in Spintronics, Core Research Cluster, Tohoku University, Sendai 980-8577, Japan

[a)]**Author to whom correspondence should be addressed:** itok@imr.tohoku.ac.jp

## ABSTRACT

$L1_0$-orderd FeNi alloy films with a high degree of order ($S$) and a large uniaxial magnetic anisotropy energy ($K_u$) were realized by denitriding FeNiN films. FeNiN films with the $a$-axis perpendicular to the film plane were epitaxially grown on $SrTiO_3$ (001) substrates by molecular beam epitaxy by changing the growth temperatures ($T_S$) to 200, 250, and 350 °C. The $a$-axis oriented epitaxial $L1_0$-FeNi films were fabricated by annealing the FeNiN films in a $H_2$ gas atmosphere at 300 °C. $S$ and $K_u$ of the denitrided $L1_0$-FeNi films were characterized by anomalous x-ray diffraction using synchrotron radiation and magnetic torque measurements, respectively. A high $S$ of 0.87 and a $K_u$ of $5.9 \times 10^5$ J/m$^3$ were realized in the $L1_0$-FeNi film with a $T_S$ of 350 °C. This high $S$ value exceeds the values reported on $L1_0$-FeNi to date, but the $K_u$ value was comparable to those of $c$-axis oriented $L1_0$-FeNi films with $S \sim 0.5$ grown by alternate monoatomic deposition of Fe and Ni layers. A possible origin for the suppressed macroscopic $K_u$ in $a$-axis oriented $L1_0$-FeNi films is discussed, and denitriding FeNiN is a promising method for the fabrication of $L1_0$-FeNi with a high $S$ and a large $K_u$.



In recent years, ferromagnetic materials for permanent magnets have actively been investigated due to an increase demand for application in high efficiency motors of electric vehicles. For permanent magnets, ferromagnetic materials with high saturation magnetization ($M_S$) and large uniaxial magnetic anisotropy energy ($K_u$) are required. However, typical ferromagnetic materials with a large $K_u$ contain rare earth elements or noble metal elements[1] and the development of ferromagnetic materials without such elements is required to realize a sustainable society. We have been interested in an $L1_0$-ordered FeNi alloy as a high $M_S$ and large $K_u$ material suitable for application in rare earth- and noble metal-free permanent magnets.[2] $L1_0$-FeNi possesses a face-centered tetragonal structure with alternate stacking of Fe and Ni monatomic layers along the $c$-axis direction. An $M_S$ of 1270 kA/m, a $K_u$ of $1.3 \times 10^6$ J/m$^3$,[3,4] and a Curie temperature of 550 °C (Refs. 5 and 6) were reported in a bulk form $L1_0$-FeNi. The order-disorder transition temperature of $L1_0$-FeNi is 320 °C,[3,7,8] and the $L1_0$ phase is obtained by annealing disordered FeNi alloys below this temperature in theory. However, 320 °C is too low to promote the diffusion of Fe and Ni atoms sufficiently and it takes astronomical time to obtain the $L1_0$ phase.

The bulk form of $L1_0$-FeNi was fabricated by special methods such as heat treatment for disordered FeNi alloys with neutron irradiation,[3,4] severe plastic deformation for FeNi powder,[9] and annealing of amorphous FeNiSiBPCu alloys produced by rapid quench.[10] However, the volume fraction or the degree of long-range order ($S$) of the $L1_0$ phase was small for these samples.

We have focused on the fabrication of $L1_0$-FeNi films and the improvement of their $S$ and $K_u$.[2] Epitaxially grown $L1_0$-FeNi films with the $c$-axis perpendicular to the film plane were fabricated by alternate monoatomic deposition of Fe and Ni layers on Au–Cu–Ni buffer layers using molecular beam epitaxy (MBE).[11] An $S$ of ~0.5 and a $K_u$ of $7.0 \times 10^5$ J/m$^3$ were realized and a $K_u$ exceeding $10^6$ J/m$^3$ could be expected if $S$ larger than 0.7 is achieved.[11] X-ray magnetic circular dichroism measurements were performed for the $c$-axis oriented $L1_0$-FeNi films, and it is revealed that the uniaxial magnetic anisotropy of $L1_0$-FeNi is largely dominated by the anisotropy of the Fe orbital magnetic moment.[12] This result is consistent with the prediction by the first-principles calculation.[13] In addition to the MBE method, the combination of sputtering deposition and rapid thermal annealing,[14,15] and the fabrication by pulsed laser deposition were also performed.[16] However, $S$ and $K_u$ exceeding those reported in Ref. 11 were not realized.

On the other hand, we synthesized $L1_0$-FeNi powder with an $S$ of 0.71 by extracting nitrogen atoms from antiferromagnetic tetragonal FeNiN powder,[17] where FeN and Ni monoatomic layers are alternately stacked in the $c$-axis direction due to the higher affinity of Fe–N bonds than that of Ni–N bonds,[18–22] by the annealing in a $H_2$ gas atmosphere while maintaining the Fe/Ni ordered structure. A coercivity of 142 kA/m was achieved in the $L1_0$-FeNi powder but its $K_u$ value was not evaluated because of its polycrystalline form. In order to demonstrate the advantage of $L1_0$-FeNi produced by the denitriding method in permanent magnet applications, the fabrication of epitaxial $L1_0$-FeNi films by denitriding single-crystal-like FeNiN films would be useful to characterize their $K_u$ and $S$.

In this study, FeNiN films with the $a$-axis perpendicular to the film plane with two variants were epitaxially grown on $SrTiO_3$ (STO) (001) substrates and denitrided, leading to the realization of a high $S$ of 0.87 and a large $K_u$ of $5.9 \times 10^5$ J/m$^3$ in $a$-axis oriented $L1_0$-FeNi films. This high $S$ value exceeds the values reported previously.[2,10,11,16,17]

20 nm-thick FeNiN films were grown by the simultaneous supply of Fe, Ni, and radio frequency $N_2$ by MBE[23,24] by changing the growth temperature ($T_S$) to 200, 250, and 350 °C. After the growth, the FeNiN films were annealed at 300 °C for 4 h in a furnace with a 1.0 l/min $H_2$ gas flow rate for denitriding, resulting in the fabrication of $L1_0$-FeNi films. The thicknesses of the $L1_0$-FeNi films were estimated by x-ray reflectometry. The structure of the FeNiN films was characterized by out-of-plane and in-plane x-ray diffraction (XRD) measurements using Cu $K\alpha$ radiation. In addition, in-plane anomalous XRD measurements were performed for the $L1_0$-FeNi films at a synchrotron radiation facility, BL46XU of SPring-8 in Japan, in order to observe the superlattice diffraction attributed to the Fe-Ni long range order. A scattering vector ($\boldsymbol{Q}$) was set to STO[100] and the incident photon energy was 7.11 keV, which corresponds to the absorption edge of Fe. $S$ of the $L1_0$-FeNi films was evaluated by using the integrated peak intensities of observed fundamental and superlattice diffraction and those of theoretically calculated. The details of the procedure for deriving $S$ are summarized in Ref. 15. The Fe/Ni composition ratios of the samples were confirmed by the combination of Rutherford backscattering spectrometry and electron probe micro analyzer analysis as $Fe_{51}Ni_{49}$ for the samples of $T_S$ of 200 and 250 °C and $Fe_{52}Ni_{48}$ for $T_S$ of 350 °C. They were taken into account to calculate the $S$ values.[25] Cross-sectional scanning transmission electron microscope (STEM) measurements with fast Fourier transform (FFT) analysis were performed for the $L1_0$-FeNi films and the size of variants in them was roughly estimated. Magnetization curves were measured by a vibrating sample magnetometer with external magnetic fields ($H$) applied along the in-plane STO[100] or the out-to-plane STO[001] direction at room temperature (RT). $M_S$ and $K_u$ were evaluated by magnetic torque measurements with so-called the 45° method.[26] Torque curves were measured at RT under $H$ with rotating the electromagnet clockwise and counterclockwise around the STO(010) plane of the samples as shown in the inset of Fig. 3(a).[24]

Figures 1(a) and 1(b) show the out-of-plane and in-plane XRD patterns of the FeNiN films, respectively, measured by using Cu $K\alpha$ radiation. They indicate the $a$-axis oriented epitaxial growth along the perpendicular direction to the film plane with two variants: the epitaxial relationships are FeNiN[001](100)//STO[100](001) and FeNiN[010](100)//STO[100](001) as shown schematically in Fig. 1(c).[23,24] In other words, the two variants with the in-plane $c$-axis of FeNiN intersecting at 90° were formed indicated by variants A and B in Fig. 1(c). At present, the reason for the $a$-axis orientation perpendicular to the film plane is not clear. As for the samples with a $T_S$ of 250 and 350 °C, the superlattice peaks of FeNiN 001, which are attributed to the long-range order of N atoms in FeNiN, are clearly observed in the in-plane XRD patterns.

Figures 1(d) and 1(e) display the in-plane anomalous XRD patterns of the $L1_0$-FeNi films after denitriding the FeNiN films obtained by using the synchrotron radiation with a photon energy of 7.11 keV. Figure 1(d) show the patterns with the $2\theta$ range from 22° to 32° and Fig. 1(e) from 54° to 60°. The overlapped fundamental diffraction peaks of $L1_0$-FeNi 200 + 002 are observed in Fig. 1(e) because the $c/a$ ratio of $L1_0$-FeNi is close to 1.0, and the epitaxial relationship between the $L1_0$-FeNi films and the STO(001) substrates is maintained after denitriding. The peak intensity increases with $T_S$ and the clear superlattice diffraction of $L1_0$-FeNi 001 is obtained for $T_S = 350$ °C as shown in Fig. 1(d). This peak disappeared when the incident x-ray energy was changed from 7.11 keV, which is the proof of the superlattice diffraction of $L1_0$-FeNi. $S$ for $T_S = 350$ °C is calculated to be 0.87 using the equation

$$S = \sqrt{\frac{I_{001}^{obs}/I_{002}^{obs}}{I_{001}^{cal}/I_{002}^{cal}}}, \quad (1)$$

where $I_{001}^{obs}$ and $I_{002}^{obs}$ are the integrated intensities of observed diffraction peaks for $L1_0$-FeNi 001 (superlattice) and $L1_0$-FeNi 002 (fundamental), respectively. $I_{001}^{cal}$ and $I_{002}^{cal}$ are theoretically calculated intensities when $S = 1$ likewise. This $S$ value exceeds those of the $c$-axis oriented $L1_0$-FeNi films ($S \sim 0.5$) grown by alternate monoatomic deposition of Fe and Ni layers[11] and the $L1_0$-FeNi powder ($S = 0.71$) fabricated by denitriding FeNiN powder.[17] For the evaluation of $S$, we separated the overlapped peak of $L1_0$-FeNi 200 + 002 into $L1_0$-FeNi 200 and 002 using the following equation:

$$I_{200(002)}^{obs} = I_{200+002}^{obs} \times I_{200(002)}^{cal} / \left( I_{200}^{cal} + I_{002}^{cal} \right). \quad (2)$$

We assume that the two variants have the same volume fraction because of the symmetry in the STO(001) plane.

Figure 2 indicates the magnetization curves of the $L1_0$-FeNi films with the in-plane and out-of-plane $H$. The $M_S$ values are approximately 1100 kA/m for all the samples. The coercivity of the samples is

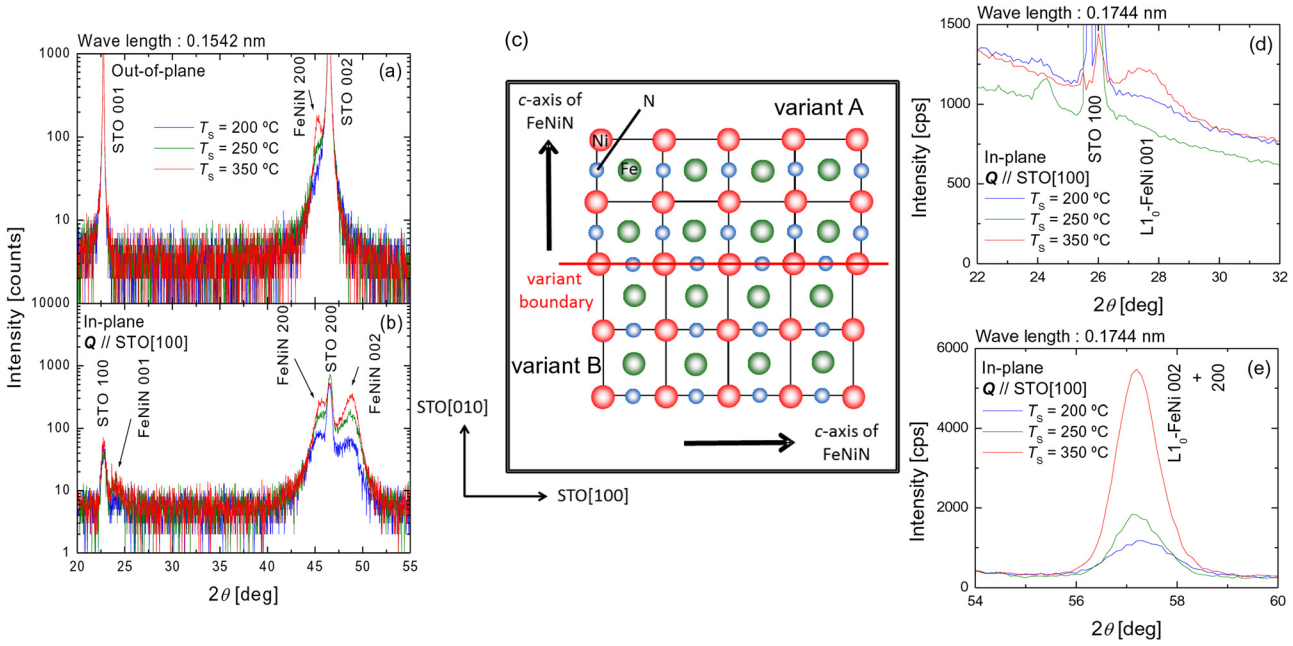


**FIG. 1.** (a) Out-of-plane and (b) in-plane XRD patterns of FeNiN films measured by using Cu $K\alpha$ radiation. (c) A schematic illustration of the structure of epitaxially grown FeNiN films with the *a*-axis perpendicular to the film plane with two variants on an STO(001) substrate. The atomic arrangement at the boundary between variants shown here (—Ni–N–Ni–) is an example. (d) and (e) In-plane anomalous XRD patterns of $L1_0$-FeNi films measured by using synchrotron radiation with a photon energy of 7.11 keV.

small (~0.01 T) in the in-plane magnetization curves but single-crystal-like, continuous films often show low coercivity even in the case of high magnetic anisotropy because of a low density of pinning sites for domain walls.[27] For the in-plane magnetization curves, the remanent magnetization is smaller than $M_S$. This is attributed to the presence of the *a*-axis, i.e., the hard magnetization axis, of $L1_0$-FeNi in the in-plane direction of the samples. Furthermore, for the out-of-plane magnetization curves, the saturation fields of the samples are larger than the demagnetization field (~1.4 T). This is attributed to the *a*-axis, i.e., the hard magnetization axis, perpendicular to the film plane. These features of the magnetization curves are explained by the microstructure having two variants with orthogonal in-plane *c*-axes, i.e., the easy magnetization axis, from each other, showing uniaxial magnetic anisotropy for each. The decrease in remanent magnetization in the in-plane magnetization curves and the increase in saturation field in the out-of-plane magnetization curves with $T_S$ mean the enhancement of $K_u$ with $T_S$.

Figure 3(a) exhibits the magnetic torque ($L$) measurements with the 45° method,[26] i.e., $L$ vs $(L/\mu_0 H)^2$ plots, for the $L1_0$-FeNi films. $\mu_0$ is the permeability in a vacuum. $M_S$ and effective uniaxial magnetic anisotropy energy ($K_u^{eff}$) were obtained from the intersections of the fitting lines with the vertical and horizontal axes, respectively, from the following equation:[26]

$$\left(\frac{L}{\mu_0 H}\right)^2 = -\frac{M_S^2}{2K_u^{eff}} L + \frac{M_S^2}{2}. \tag{3}$$

By considering the two variants of the samples with the in-plane *c*-axes orthogonal to each other, magnetic anisotropy energy ($E_A$) is expressed by

$$E_A = K_u^{eff} \sin^2\varphi_B = \frac{1}{2}\cdot\frac{\mu_0 M_S^2}{2}\cdot \sin^2\varphi_B + \frac{1}{2}\left(K_u + \frac{\mu_0 M_S^2}{2}\right)\sin^2\varphi_B$$
$$= \left(\frac{K_u + \mu_0 M_S^2}{2}\right)\sin^2\varphi_B. \tag{4}$$

Here, $\frac{1}{2}\cdot\frac{\mu_0 M_S^2}{2}\cdot\sin^2\varphi_B$ and $\frac{1}{2}\left(K_u + \frac{\mu_0 M_S^2}{2}\right)\sin^2\varphi_B$ terms in Eq. (4) correspond to $E_A$ from variants A and B, respectively, assuming that the

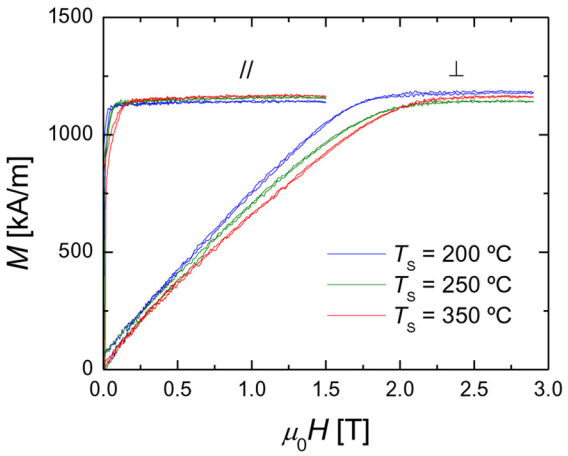


**FIG. 2.** Magnetization curves of *a*-axis oriented $L1_0$-FeNi films. Magnetic field $H$ was applied along the in-plane (//) or out-of-plane (⊥) direction. $\mu_0$ is the permeability in a vacuum.

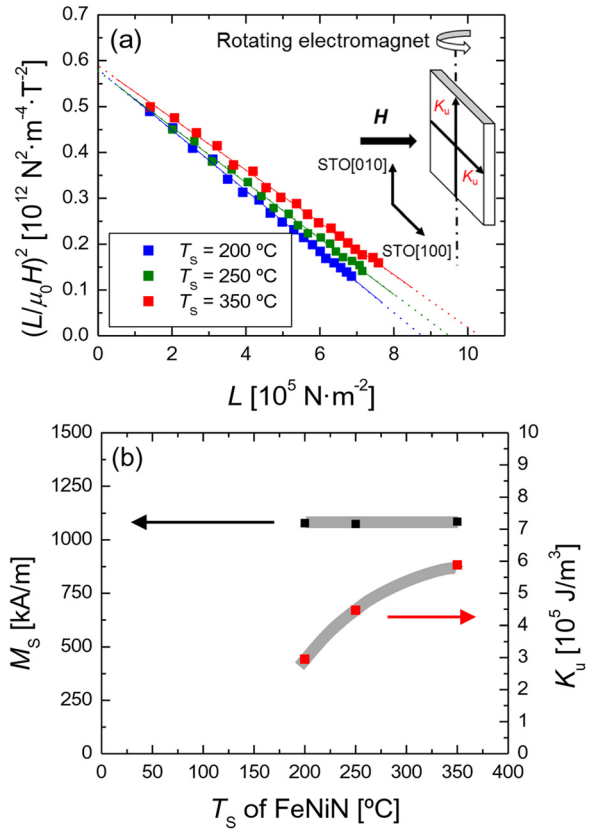


**FIG. 3.** (a) $L$ vs $(L/\mu_0 H)^2$ plots of $a$-axis oriented $L1_0$-FeNi films, where $L$ and $H$ are the magnetic torque and applied magnetic field, respectively. The inset shows the geometry of the film sample and $H$. (b) $T_S$ dependences of $M_S$ and $K_u$ of the samples.

two variants have the same volume fraction. In this paper, a positive $K_u$ means that the easy magnetization axis direction of the film is in-plane. We define $\varphi_A$ and $\varphi_B$ as the angles between $M_S$ and $c$-axis of variants A and B, respectively. Due to the sample setup of the magnetic torque measurements as shown in the inset of Fig. 3(a), for the variant A, its $c$-axis and the magnetization are always orthogonal ($\varphi_A = 90°$). This means that the $K_u$ component in the variant A does not affect the measurements but only the shape magnetic anisotropy term ($\mu_0 M_S^2/2$) does. On the other hand, for the variant B, the magnetization rotates in the range of $\varphi_B = -90°$ to 90° with respect to the easy axis for the magnetocrystalline anisotropy, which is the same situation as for the shape magnetic anisotropy. Therefore, both the magnetocrystalline and the shape magnetic anisotropies are detected by the torque measurements and described as $K_u + \mu_0 M_S^2/2$. Using the equation

$$K_u = 2\left(K_u^{\mathrm{eff}} - \frac{\mu_0 M_S^2}{2}\right), \tag{5}$$

the $K_u$ value is calculated. Figure 3(b) shows the $T_S$ dependences of $M_S$ and $K_u$ of the samples evaluated by the magnetic torque measurements. The $M_S$ values are almost constant at approximately 1100 kA/m and they are consistent with the magnetization measurements, which supports the reliability of the fitting in Fig. 3(a). The $K_u$ value increases with $T_S$ of the FeNiN layers and reaches $5.9 \times 10^5$ J/m$^3$ at $T_S = 350$ °C. This $K_u$ value approaches that of the $c$-axis oriented $L1_0$-FeNi films fabricated by alternate monoatomic deposition of Fe and Ni layers, $K_u = 7.0 \times 10^5$ J/m$^3$ when $S \sim 0.5$.[11] However, considering the large $S$ of 0.87 in our sample, $K_u$ should be larger than that of the $L1_0$-FeNi films in Ref. 11. A possible origin for the small $K_u$ is that the macroscopic $K_u$ of the $a$-axis oriented $L1_0$-FeNi films is suppressed by the exchange coupling between the two variants with the orthogonal in-plane $c$-axes.

In order to estimate the variant sizes, the cross-sectional STEM observations were performed for the $L1_0$-FeNi film with $S = 0.87$ and the observed images are shown in Fig. 4(a). The incident electron beam direction was set to STO[100], which corresponds to the $L1_0$-FeNi[001] or [100] direction of the film. The clear lattice images of the

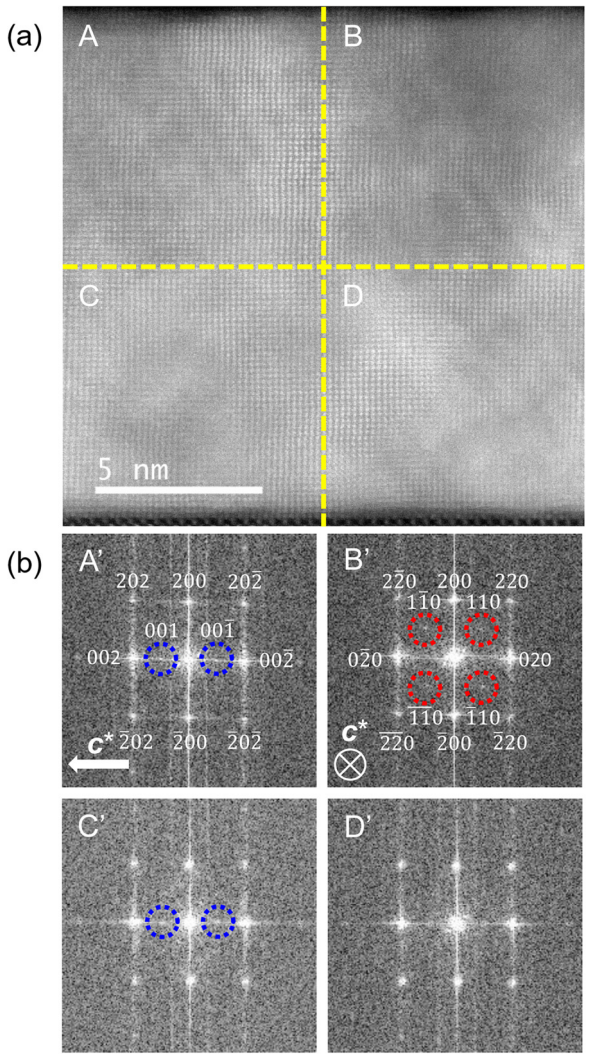


**FIG. 4.** (a) Cross-sectional STEM images and (b) their FFT images of the $a$-axis oriented $L1_0$-FeNi film with $S = 0.87$. Superlattice diffraction spots are represented by red and blue dashed circles in (b). The $c^*$ with arrows in (b) represent the directions of reciprocal lattice vectors for the $c$-axes.

epitaxially grown $L1_0$-FeNi film were obtained. Figure 4(b) exhibits the FFT images of Fig. 4(a), where panels A′–D′ correspond to the FFT images of areas A–D in Fig. 4(a). From area D, no superlattice diffraction was observed, which means that $S$ is locally degraded or multiple domains overlap in the electron beam transmission direction. On the other hand, the superlattice diffractions, represented by red and blue dashed circles in Fig. 4(b), are definitely observed in areas A, B, and C. The difference of the spot positions between the red and blue dashed circles indicates the different variants of the $L1_0$-FeNi film. Observation positions were also changed, and the variant sizes were roughly estimated to be a few nanometers.

Here, we discuss the effect of the variants with the easy magnetization axes intersecting at 90°, on the macroscopic $K_u$ values of $a$-axis oriented $L1_0$-FeNi films. The relationship between the crystal grain size, the macroscopic magnetic anisotropy energy, and the coercivity of nanocrystalline ferromagnetic films in which the magnetic easy axis direction is random was reported by Herzer.[28] The macroscopic $K_u$ value may be averaged and becomes smaller than the $K_u$ of each crystal grain when the crystal grain size is smaller than the exchange length ($L_{ex}$), which is described as

$$L_{ex} = \sqrt{\frac{A}{K_u}}. \quad (6)$$

$A$ is the exchange stiffness constant. Our $L1_0$-FeNi films are not nanocrystalline but a mixture consisting of the two nanometer-sized variants with orthogonal easy magnetization axes, showing a similar situation to that of nanocrystalline ferromagnetic films. The $A$ of $L1_0$-FeNi is $1.0 \times 10^{-11}$ J/m,[29] and $L_{ex}$ is estimated to be 3.2 nm when we assume a $K_u$ of $1 \times 10^6$ J/m$^3$. Thus, the $L_{ex}$ of $L1_0$-FeNi is comparable to the variant sizes of our samples. This strongly suggests that the obtained macroscopic $K_u$ values of $a$-axis oriented $L1_0$-FeNi films may be smaller than the actual $K_u$ of each variant.

In summary, $a$-axis oriented $L1_0$-FeNi films with a high $S$ and a large $K_u$ were fabricated by denitriding $a$-axis oriented FeNiN films. As a result of denitriding, FeNiN films prepared at $T_S = 350$ °C, $S = 0.87$, and $K_u = 5.9 \times 10^5$ J/m$^3$ were realized. This $S$ value is higher than those reported on $L1_0$-FeNi previously.[2,10,11,16,17] However, the $K_u$ value is smaller than that expected from the previous study on the $c$-axis oriented $L1_0$-FeNi films by alternate monoatomic deposition.[11] A possible origin for the small $K_u$ is that the microstructure having two nanometer-sized variants with the in-plane $c$-axes orthogonal to each other, resulting in the reduction of the macroscopic $K_u$ value. The actual $K_u$ of each variant may be much larger than $5.9 \times 10^5$ J/m$^3$.

We thank H. Onoda and T. Sekido, University of Tsukuba, for their support with the magnetic torque experiments. This work was supported by the Future Pioneering Program "Development of magnetic material technology for high-efficiency motors" (Proposal No. JPNP14015) commissioned by the New Energy and Industrial Technology Development Organization (NEDO), Japan. The conventional XRD measurements and EPMA analysis were carried out at the Cooperative Research and Development Center for Advanced Materials (CRDAM), Institute for Materials Research, Tohoku University (Proposal Nos. 18G0409 and 19G0402). The synchrotron radiation XRD measurements were conducted at the BL46XU of SPring-8 with the approval of JASRI (Proposal No. 2019A1802). The STEM measurements were supported by the Tohoku University Microstructural Characterization Platform in Nanotechnology Platform Project sponsored by the Ministry of Education, Culture, Sports, Science and Technology (MEXT), Japan (Proposal No. JPMX09F-A-19-TU-0018).

## DATA AVAILABILITY

The data that support the findings of this study are available from the corresponding author upon reasonable request.

## REFERENCES

[1]J. M. D. Coey, IEEE Trans. Magn. **47**, 4671 (2011).
[2]K. Takanashi, M. Mizuguchi, T. Kojima, and T. Y. Tashiro, J. Phys. D **50**, 483002 (2017).
[3]L. Néel, J. Paulevé, R. Pauthenet, J. Laugier, and D. Dautreppe, J. Appl. Phys. **35**, 873 (1964).
[4]J. Paulevé, A. Chamberod, K. Krebs, and A. Bourret, J. Appl. Phys. **39**, 989 (1968).
[5]T. Nagata and M. Funaki, Mem. Natl. Inst. Polar Res. **46**, 245 (1987).
[6]P. Wasilewski, Phys. Earth Planet. Inter. **52**, 150 (1988).
[7]K. B. Reuter, D. B. Williams, and J. I. Goldsteine, Metall. Trans. A **20**, 711 (1989).
[8]M. Uehara, J. Gattacceca, H. Leroux, D. Jacob, and C. J. van der Beek, Earth Planet. Sci. Lett. **306**, 241 (2011).
[9]S. Lee, K. Edalati, H. Iwaoka, Z. Horita, T. Ohtsuki, T. Ohkochi, M. Kotsugi, T. Kojima, M. Mizuguchi, and K. Takanashi, Philos. Mag. Lett. **94**, 639 (2014).
[10]A. Makino, P. Sharma, K. Sato, A. Takeuchi, Y. Zhang, and K. Takenaka, Sci. Rep. **5**, 16627 (2015).
[11]T. Kojima, M. Mizuguchi, T. Koganezawa, K. Osaka, M. Kotsugi, and K. Takanashi, Jpn. J. Appl. Phys., Part 1 **51**, 062601 (2012).
[12]M. Kotsugi, M. Mizuguchi, S. Sekiya, M. Mizumaki, T. Kojima, T. Nakamura, H. Osawa, K. Kodama, T. Ohtsuki, T. Ohkochi, K. Takanashi, and Y. Watanabe, J. Magn. Magn. Mater. **326**, 235 (2013).
[13]Y. Miura, S. Ozaki, Y. Kuwahara, M. Tsujikawa, K. Abe, and M. Shirai, J. Phys. **25**, 106005 (2013).
[14]T. Y. Tashiro, M. Mizuguchi, T. Kojima, T. Koganezawa, M. Kotsugi, T. Ohtsuki, and K. Takanashi, J. Appl. Phys. **117**, 17E309 (2015).
[15]T. Y. Tashiro, M. Mizuguchi, T. Kojima, T. Koganezawa, M. Kotsugi, T. Ohtsuki, K. Sato, T. Konno, and K. Takanashi, J. Alloys Compd. **750**, 164 (2018).
[16]M. Saito, H. Ito, Y. Suzuki, M. Mizuguchi, T. Koganezawa, T. Miyamachi, F. Komori, K. Takanashi, and M. Kotsugi, Appl. Phys. Lett. **114**, 072404 (2019).
[17]S. Goto, H. Kura, E. Watanabe, Y. Hayashi, H. Yanagihara, Y. Shimada, M. Mizuguchi, K. Takanashi, and E. Kita, Sci. Rep. **7**, 13216 (2017).
[18]R. J. Arnott and A. Wold, J. Phys. Chem. Solids **15**, 152 (1960).
[19]S. Goto, H. Kura, H. Yanagihara, E. Kita, M. Tsujikawa, R. Sasaki, M. Shirai, Y. Kobayashi, T. Honda, and K. Ono, ACS Appl. Nano Mater. **2**, 6909 (2019).
[20]S. Goto, H. Kura, and H. Yanagihara, J. Magn. Soc. Jpn. **44**, 75 (2020).
[21]W. B. Mi, E. Y. Jiang, and H. L. Bai, J. Appl. Phys. **99**, 034315 (2006).
[22]V. Phatak, A. Gupta, V. R. Reddy, S. Chakravarty, H. Schmidt, and R. Rüffer, Acta Mater. **58**, 979 (2010).
[23]F. Takata, K. Ito, and T. Suemasu, Jpn. J. Appl. Phys., Part 1 **57**, 058004 (2018).
[24]K. Ito, M. Hayashida, M. Mizuguchi, T. Suemasu, H. Yanagihara, and K. Takanashi, J. Magn. Soc. Jpn. **43**, 79 (2019).
[25]T. Kojima, M. Ogiwara, M. Mizuguchi, M. Kotsugi, T. Koganezawa, T. Ohtsuki, T. Y. Tashiro, and K. Takanashi, J. Phys. **26**, 064207 (2014).
[26]H. Miyajima, K. Sato, and T. Mizoguchi, J. Appl. Phys. **47**, 4669 (1976).
[27]T. Shima, K. Takanashi, Y. K. Takahashi, and K. Hono, Appl. Phys. Lett. **81**, 1050 (2002).
[28]G. Herzer, IEEE Trans. Magn. **26**, 1397 (1990).
[29]M. Kotsugi, C. Mitsumata, H. Maruyama, T. Wakita, T. Taniuchi, K. Ono, M. Suzuki, N. Kawamura, N. Ishimatsu, and M. Oshima, Appl. Phys. Express **3**, 013001 (2010).